# Self-assembled $Mn_5Ge_3$ nanomagnets close to the surface and deep inside a $Ge_{1-x}Mn_x$ epilayer

R. T. Lechner,[1,a)] V. Holý,[2] S. Ahlers,[3] D. Bougeard,[3] J. Stangl,[1] A. Trampert,[4] A. Navarro-Quezada,[1] and G. Bauer[1]
[1]*Institut für Halbleiter-und Festkpörperphysik, Johannes Kepler Universität Linz, 4040 Linz, Austria*
[2]*Faculty of Mathematics and Physics, Charles University, Ke Karlovu 5, 121 16 Prague, Czech Republic*
[3]*Walter Schottky Institut, Technische Universität München, D-85748 Garching, Germany*
[4]*Paul Drude Institut für Festkörperelektronik, Hausvogteipl. 5-7, D-10117 Berlin, Germany*

(Received 17 April 2009; accepted 5 June 2009; published online 13 July 2009)

Under defined growth conditions ferromagnetic hexagonal $Mn_5Ge_3$ precipitates are formed in cubic $Ge_{1-x}Mn_x$ epilayers. To study the topotaxial relationship of these nanomagnets we perform x-ray diffraction experiments in coplanar as well as in grazing incidence geometries at synchrotron sources. Additionally, to the well defined topotaxial relation derived for buried nanomagnets deep within the Ge layer, we found an additional class of $Mn_5Ge_3$ precipitates very close to the surface, with larger inclusion diameter and several different crystallographic orientations with respect to the buried ones. © *2009 American Institute of Physics*. [DOI: 10.1063/1.3159827]

For future spintronic applications diluted magnetic semiconductors (DMS) (Ref. 1) with a compatibility to the mature Si technology could play an important role. $Ge_{1-x}Mn_x$ is most probably the so far best investigated system in this respect grown either on Ge substrates[2–12] or directly on Si wafers.[13] The magnetic properties of $Ge_{1-x}Mn_x$ layers with a small Mn content of few percent are substantially influenced by inhomogeneities of the distribution of Mn atoms in the Ge host lattice. Depending on the substrate temperature during molecular beam epitaxial (MBE) growth, coherent cubic Mn-rich clusters[7,14] or ferromagnetic hexagonal $Mn_5Ge_3$ precipitates can occur.[6,14] Ways leading to a controlled formation[1] and alignment of these nanomagnets embedded in a nonmagnetic semiconductor matrix will be necessary to tune the magnetic properties of the whole DMS.

In this letter, we investigate orientation, location, and dimensions of $Mn_5Ge_3$ precipitates embedded in a crystalline, cubic $Ge_{1-x}Mn_x$ matrix by combining synchrotron x-ray diffraction (XRD) in grazing incidence (GID) as well as coplanar geometry (CoXRD) with transmission electron microscopy (TEM). From GID we deduce the average diameter of the precipitates depth sensitive and obtain information on their in-plane orientation. From CoXRD we derive the inclusion parameters along the Ge $[001]_{Ge}$ direction; both geometries allow to determine the alignment accuracy of the hexagonal $Mn_5Ge_3$ precipitates along the cubic directions.

The 200 nm thin $Ge_{1-x}Mn_x$ epilayers investigated were grown by MBE on a Ge (001) substrate with a Mn content of 3.4% and a Ge flux rate of 0.08 Å/s at a substrate temperature of 120 °C. Growth details can be found in Ref. 6. The XRD experiments were carried out at the beamlines ID01 for GID and ID31 for CoXRD at the European Synchrotron Radiation Facility (ESRF) using x-ray wavelengths of 1.9 and 0.8 Å, respectively. In GID the scattered intensity was measured by a linear detector perpendicular to the sample surface. During the measurements the incidence angle $\alpha_i$ of the primary radiation was kept constant. $\alpha_i$ was chosen to be 0.32°, i.e., slightly below the critical angle $\alpha_c$ of the total external reflection (0.38° for the energy used), or $\alpha_i$=0.45°, yielding a penetration depth $D_{pen}$ of ~10 nm and 1 μm, respectively. The scattered intensity was measured along lines crossing the in-plane reciprocal lattice points (RLPs) (220) or (400) of Ge; these lines were parallel ($q_r$) and perpendicular ($q_a$) to the corresponding diffraction vectors, i.e., radial and angular intensity scans, respectively.

In Fig. 1 such scans reveal peaks additional to cubic Ge RLPs at positions, which fit to the positions of bulk $Mn_5Ge_3$ RLPs as calculated from the $Mn_5Ge_3$ lattice constants[15] $a_{hex}$=7.184 Å and $c_{hex}$=5.053 Å. These RLPs are therefore attributed to the presence of $Mn_5Ge_3$ precipitates with a well defined topotaxial relationship to the cubic Ge lattice. In Fig. 1(a) an angular scan of the $(110)_{Mn_5Ge_3}$ peak found along the $[110]_{Ge}$ direction is shown. Here the peak intensity along $\alpha_f$ at fixed $\alpha_i$=0.45° is plotted as a function of the azimuthal angle Φ. Keeping the detector angle 2θ fixed, we rotate the

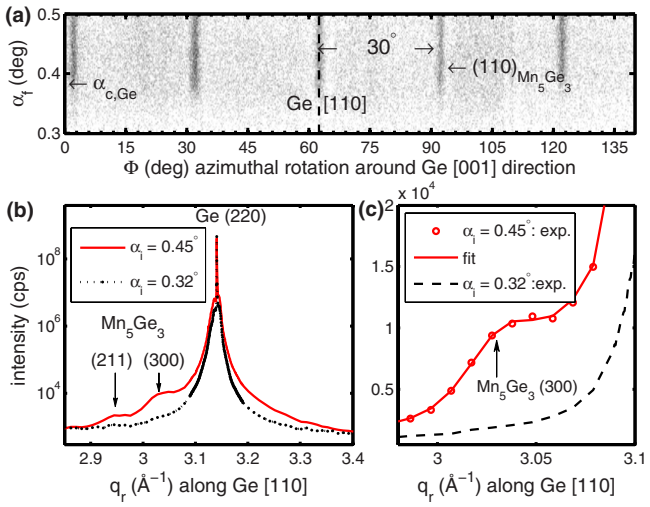


FIG. 1. (Color online) (a) Azimuthal scan of the hexagonal $(110)_{Mn_5Ge_3}$ maximum along the in-plane Ge directions. The *y*-axis shows the distribution of the peak intensities along $\alpha_f$ measured at fixed $\alpha_i$=0.45°. (b) Radial scan along $[110]_{Ge}$ at incidence angles $\alpha_i$=0.45°>$\alpha_c$ (solid line) and $\alpha_i$=0.32°<$\alpha_c$ (dotted), respectively. (c) Zoom of the region around the $(300)_{Mn_5Ge_3}$ RLPs. The solid line is a fit to the data (circles) at $\alpha_i > \alpha_c$.

a)Electronic mail: rainer.lechner@jku.at.

 

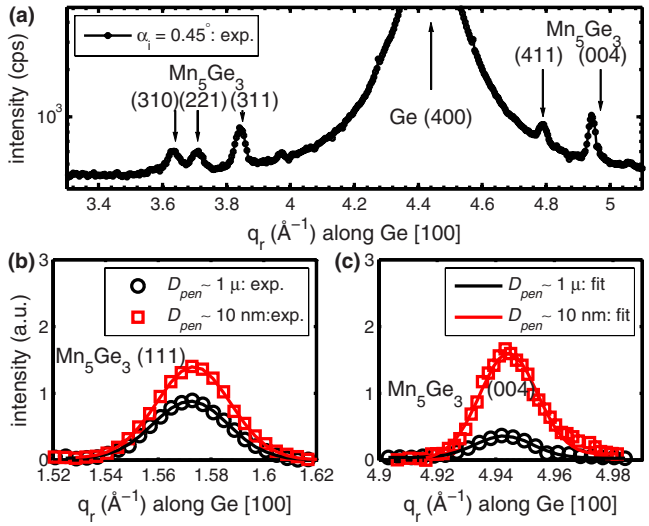


FIG. 2. (Color online) (a) Radial scan along the $[100]_{Ge}$ direction at an incidence angles $\alpha_i$=0.45° around the $(400)_{Ge}$ RLP. Several $Mn_5Ge_3$ Bragg peaks are visible. (b) Measurements (symbols) and fits (lines) of the $(111)_{Mn_5Ge_3}$ Bragg peak measured at about 10 nm (squares) and 1 $\mu$m (circles) penetration depth, respectively. The scans are normalized to the illuminated area. (c) The same as in (b), but for the $(004)_{Mn_5Ge_3}$ RLP.

sample in azimuthal direction from $[110]_{Ge}$ direction by ±70° around the $[001]_{Ge}$ surface normal. Instead of a hexagonal 60° symmetry we found a 30° one, related to two orientations mutually rotated by 30° around $[001]_{Ge}$. The $(110)_{Mn_5Ge_3}$ peak is only detectable for $\alpha_f \geq \alpha_c$. This proves that the scattered peak intensity originates from regions within the Ge layer and not from the epilayer surface. In the radial scan in Fig. 1(b), left of the Ge (220) RLP two peaks for $\alpha_i$=0.45° are visible that can be related to two $Mn_5Ge_3$ hexagonal Bragg peaks: the $(211)_{Mn_5Ge_3}$ and the $(300)_{Mn_5Ge_3}$, respectively. The position of the $(300)_{Mn_5Ge_3}$ peak is located in the $[110]_{Ge}$ direction, which reveals that the $(100)_{Mn_5Ge_3}$ plane is parallel to the $(110)_{Ge}$ plane, while the $(001)_{Mn_5Ge_3}$ plane is parallel to $(001)_{Ge}$, i.e., the $c_{hex}$-axis is parallel to the $[001]_{Ge}$ direction. With the 30° periodicity obtained from the angular scan of Fig. 1(a), there are therefore two equivalent in-plane orientations of the precipitates exhibiting an angle between the $Mn_5Ge_3$ $a_{hex}$-axis and the $[110]_{Ge}$ direction of either 0° or 30°. These two orientations correspond to the lattice plane relations $(100)_{Mn_5Ge_3} \| (110)_{Ge}$ or $(110)_{Mn_5Ge_3} \| (110)_{Ge}$, which confirm and extend the topotaxial relationship obtained in previously performed TEM studies,[6] namely, $[110]_{Mn_5Ge_3} \| [110]_{Ge}$.

For $\alpha_i$=0.32°, i.e., $D_{pen}$~10 nm, the $(300)_{Mn_5Ge_3}$ vanishes in Fig. 1(b) and in the close-up Fig. 1(c). Thiscan be only explained by precipitates located more than 10 nm away from the layer surface, which is also confirmed by TEM studies, where $Mn_5Ge_3$ precipitates were found only close to the Ge-layer-Ge-substrate interface.[6,14] These are denoted as *buried* precipitates.

The $(211)_{Mn_5Ge_3}$ peak, in contrast, is visible both in the $\alpha_i$=0.45° and faintly in the $\alpha_i$=0.32° scan of Fig. 1(b). The presence of this peak for both values of $\alpha_i$ indicates the presence of an additional orientation either of buried precipitates, or of precipitates located close to the epilayer surface.

Even more precipitate orientations were found in radial GID scans along the in-plane $[100]_{Ge}$ direction as shown in Fig. 2. Several different topotaxial relationships were found. The (310), (221), (311), (411), and (004) RLPs in Fig. 2(a) as well as the (111) RLP [see Fig. 2(b)] are fingerprints for $Mn_5Ge_3$ precipitates with various inclined orientations with respect to the Ge host lattice. From the $(310)_{Mn_5Ge_3}$ RLP, e.g., we found that the $[100]_{Mn_5Ge_3}$ direction makes an in-plane angle of 43.9° with $[100]_{Ge}$, whereas the $c_{hex}$-axis is parallel to $[001]_{Ge}$. From the $(111)_{Mn_5Ge_3}$ RLP we can determine that the $c_{hex}$-axis of this class of precipitates is inclined by 35.1° to $[001]_{Ge}$. The $(004)_{Mn_5Ge_3}$ RLP in Figs. 2(a) and 2(c), for instance, originates from precipitates with $c_{hex}$-axis $\perp$ to the $[001]_{Ge}$ direction, i.e., tilted by 90° with respect to the buried precipitates. The detected RLP positions are in good agreement with the calculated positions marked by the arrows in Fig. 2(a). Thus, there is strong evidence for only one single structural species of precipitates, i.e., $Mn_5Ge_3$, within the Ge layer but depicting different orientation classes. We found no evidence for precipitates with a different crystal structure such as $Mn_{11}Ge_8$, as reported by other groups.[16–18]

The orientation classes seem to form at a different depths of the $Ge_{1-x}Mn_x$ film. From the fact that the $(111)_{Mn_5Ge_3}$ and $(004)_{Mn_5Ge_3}$ RLPs in Figs. 2(b) and 2(c) are already visible below the critical angle $\alpha_c$, i.e., at a penetration depth of only 10 nm, we deduce that these peaks originate from precipitates close to the surface. We denote these ones for brevity as *surface* precipitates. The higher intensity of these peaks at $\alpha_i$=0.32° with respect to $\alpha_i$=0.45° is related to an enhanced scattering close to $\alpha_c$.[19] The appearance of additional peaks with nonparallel RLPs could lead to the assumption of a powderlike distribution of the surface precipitates, where all crystallographic directions exist. This should result in a Debye ring along the angular direction of the RLPs. For all RLPs in Fig. 2, however, we measure a *finite* angular full width half maximum (FWHM) $\Delta\Phi$. From this we conclude that the surface precipitates can be classified by a finite, limited number of well defined crystallographic orientations with respect to the Ge lattice.

To probe orientations and sizes of all precipitates along the $[001]_{Ge}$ growth direction, i.e., along $q_z$, we record radial scans in coplanar geometry covering a large range of $q_z$ from 1.5 to ~10 Å$^{-1}$. In Fig. 3(a) the section around the $(004)_{Ge}$ RLP is shown. The arrows in Fig. 3 mark the theoretical positions of $Mn_5Ge_3$ RLPs, but only two peaks can be detected: the $(002)_{Mn_5Ge_3}$ and $(004)_{Mn_5Ge_3}$. These peaks correspond to an orientation of the $c_{hex}$-axis parallel to $[001]_{Ge}$ and are therefore attributed to the buried precipitates found in Fig. 1.

No $Mn_5Ge_3$ peaks other than those expected for buried precipitates were detected in CoXRD [see Fig. 3(a)]. Since in GID geometry a larger sample area (7 mm$^2$) is illuminated as compared to the coplanar setup (~1 mm$^2$) and due to the limited penetration depth, GID is more sensitive to precipitates close to the surface with various orientations. Hence, the signal found in the GID scans of Fig. 2(a) relates to a *minority* of precipitates and is not sufficient to be detected in CoXRD, where the diffracted intensity mainly stems from buried precipitates. The observation that precipitates form in majority as buried ones is further supported by magnetometry measurements (not shown), where the magnetic easy $c_{hex}$-axis[20] of $Mn_5Ge_3$ was found to be perpendicular to the sample surface, corresponding to a majority of buried nanomagnets with their $c_{hex}$-axis aligned $\|[001]_{Ge}$.

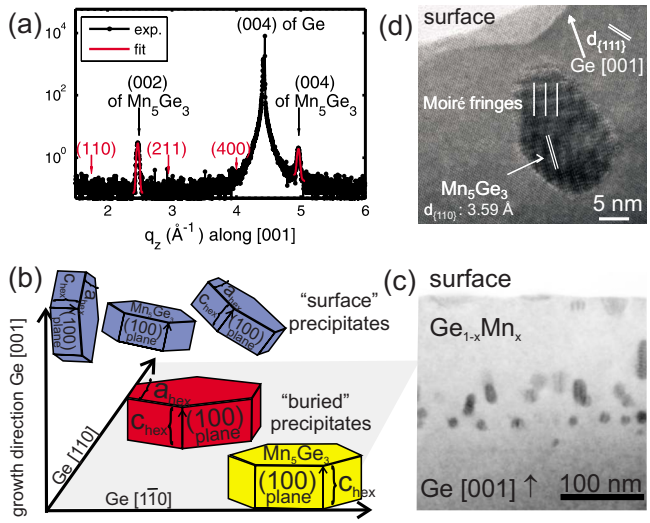


FIG. 3. (Color online) (a) Radial scan along $[001]_{Ge}$. Only two $Mn_5Ge_3$ peaks are visible: the (002) and (004). The lines are fits to the data (dots). (b) Sketch of the hexagonal $Mn_5Ge_3$ unit cells to illustrate the precipitates orientations with respect to the cubic Ge matrix. (c) TEM micrograph of the precipitates within the Ge layer. (d) HRTEM of one surface precipitate with $(110)_{Mn_5Ge_3}\|(110)_{Ge}$ but with its $c_{hex}$-axis inclined to $[001]_{Ge}$.

Indications for the presence of a majority of buried precipitates and a few surface precipitates have also been observed in TEM[6,14] [see Fig. 3(c)]. The combination of high resolution TEM (HRTEM) and the present diffraction study allows to identify surface precipitates with various orientations as sketched in the top of Fig. 3(b) and the two well defined in-plane orientations of the buried precipitates [bottom of Fig. 3(b)]. In Fig. 3(d) exemplified one HRTEM of one surface precipitate is shown with the e-beam perpendicular to $[110]_{Ge}$. The in-plane orientation is derived to $(110)_{Mn_5Ge_3}\|(110)_{Ge}$ but its $c_{hex}$-axis is inclined to $[001]_{Ge}$. Mechanisms to explain the formation of distinct buried and surface precipitate classes could be Mn diffusion toward the surface[13] and the need for a critical layer thickness[18] for incoherent precipitate nucleation.

Quantitative evaluation of the diffraction data allows to extract diameters and orientation accuracy of both buried and surface precipitates. From the FWHM of the $(300)_{Mn_5Ge_3}$ and $(110)_{Mn_5Ge_3}$ peaks in radial direction $q_r$ we get an estimate of the diameter. We found no strain broadening of the FWHMs as a function of $q_r$,[21] which is related to the fact that the formation of incoherent precipitates impose nearly no in-plane strain on the Ge-host lattice, as we have shown recently.[14] Hence, we derive from the average value of the FWHMs $\Delta q_r$ an average *in-plane* precipitate diameter with $D_{\|}=2\pi/\Delta q_r$ of $15\pm2$ nm. This value is in very good agreement with the values derived directly from TEM (Ref. 6). From the FWHMs $\Delta\Phi$ along $\Phi$, i.e., in angular direction, we estimate the accuracy of the found in-plane orientation from the mean $\Delta\Phi$ value; we derive a value of only $\sim\pm0.4°$ for the variation of the in-plane orientation of the buried precipitates. From the mean FWHM of all surface RLPs along $q_r$ in Fig. 3, we determine a mean in-plane surface inclusion diameter $D_{\|,surf}$ of $22\pm3$ nm, which is slightly larger than the corresponding value for the buried inclusions. The mean alignment accuracy within the surface orientation classes is found also to be $\sim\pm0.4°$.

From the fits of the buried $Mn_5Ge_3$ RLPs along $q_z$ we obtain a larger FWHM value for the $(004)_{Mn_5Ge_3}$ RLP with respect to the $(002)_{Mn_5Ge_3}$ RLP; hence in the [001] growth direction we observe a strain broadening of the precipitates peaks. Using a Williamson–Hall plot[21] we derive from the FWHM at $q_z=0$ an average *out-of-plane* precipitate diameter of $D_{\perp}\sim18\pm2$ nm. From the angular FWHMs perpendicular to $q_z$, we derive also the in-plane diameter $D_{\|,copl}$ and the alignment accuracy of the $c_{hex}$-axis along $[001]_{Ge}$. The value of $\sim13\pm4$ nm for $D_{\|,copl}$ is in good agreement with the determined $D_{\|}$ value of $15\pm2$ nm. The small deviation of $\pm0.55°$ from $[001]_{Ge}$ is also close to the found in-plane orientation accuracy. The diameter $D_{\perp}$ along $[001]_{Ge}$, however, is with 18 nm slightly larger than the derived in-plane values indicating an elongation along the $c_{hex}$-axis.

To conclude, using synchrotron XRD we have determined topotaxial relations of hexagonal $Mn_5Ge_3$ precipitates in a cubic $Ge_{1-x}Mn_x$ layer including the alignment accuracy of these nanomagnets. The majority of the nanomagnets belongs to a single orientation class deep within the epilayer. A minority, in contrast, resides close to the epilayer surface and is aligned in different but well defined orientation classes.

Work was supported by the Austrian Science Fund FWF (Grant No. P18942-N20), by DFG via SPP 1285, and MSM 0021620834 of the Czech Republic. The XRD experiments were performed at beamlines ID01 and ID31 (ESRF) with the help of T. H. Metzger and A. Fitch, respectively.

[1] T. Dietl and H. Ohno, Mater. Today **9**, 18 (2006).
[2] Y. D. Park, A. T. Hanbicki, S. C. Erwin, C. S. Hellberg, J. M. Sullivan, J. E. Mattson, T. F. Ambrose, A. Wilson, G. Spanos, and B. T. Jonker, Science **295**, 651 (2002).
[3] A. P. Li, C. Zeng, K. van Benthem, M. F. Chisholm, J. Shen, S. V. S. N. Rao, S. K. Dixit, L. C. Feldman, A. G. Petukhov, M. Foygel, and H. H. Weitering, Phys. Rev. B **75**, 201201(R) (2007).
[4] C. Bihler, C. Jaeger, T. Vallaitis, M. Gjukic, M. S. Brandt, E. Pippel, J. Woltersdorf, and U. Gösele, Appl. Phys. Lett. **88**, 112506 (2006).
[5] C. Jaeger, C. Bihler, T. Vallaitis, S. T. B. Goennenwein, M. Opel, R. Gross, and M. S. Brandt, Phys. Rev. B **74**, 045330 (2006).
[6] S. Ahlers, D. Bougeard, N. Sircar, G. Abstreiter, A. Trampert, M. Opel, and R. Gross, Phys. Rev. B **74**, 214411 (2006).
[7] D. Bougeard, S. Ahlers, A. Trampert, N. Sircar, and G. Abstreiter, Phys. Rev. Lett. **97**, 237202 (2006).
[8] T. Devillers, M. Jamet, A. Barski, V. Poydenot, P. Bayle-Guillemaud, E. Bellet-Amalric, S. Cherifi, and J. Cibert, Phys. Rev. B **76**, 205306 (2007).
[9] C. Zeng, Z. Zhang, K. van Benthem, M. Chisholm, and H. Weitering, Phys. Rev. Lett. **100**, 066101 (2008).
[10] J.-P. Ayoub, L. Favre, I. Berbezier, A. Ronda, L. Morresi, and N. Pinto, Appl. Phys. Lett. **91**, 141920 (2007).
[11] P. De Padova, J. P. Ayoub, I. Berbezier, P. Perfetti, C. Quaresima, A. M. Testa, D. Fiorani, B. Olivieri, J. M. Mariot, A. Taleb-Ibrahimi, M. C. Richter, O. Heckmann, and K. Hricovini, Phys. Rev. B **77**, 045203 (2008).
[12] N. Pinto, L. Morresi, M. Ficcadenti, R. Murri, F. D'Orazio, F. Lucari, L. Boarino, and G. Amato, Phys. Rev. B **72**, 165203 (2005).
[13] Y. Wang, J. Zou, Z. Zhao, X. Han, X. Zhou, and K. L. Wang, J. Appl. Phys. **103**, 066104 (2008).
[14] V. Holý, R. T. Lechner, S. Ahlers, L. Horák, T. H. Metzger, A. Navarro-Quezada, A. Trampert, D. Bougeard, and G. Bauer, Phys. Rev. B **78**, 144401 (2008).
[15] J. B. Forsyth and P. J. Brown, J. Phys.: Condens. Matter **2**, 2713 (1990).
[16] Y. D. Park, A. Wilson, A. T. Hanbicki, J. E. Mattson, T. Ambrose, G. Spanos, and B. T. Jonker, Appl. Phys. Lett. **78**, 2739 (2001).
[17] E. Biegger, L. Stäheli, M. Fonin, U. Rüdiger, and Y. S. Dedkov, J. Appl. Phys. **101**, 103912 (2007).
[18] Y. Wang, J. Zou, Z. Zhao, X. Han, X. Zhou, and K. L. Wang, Appl. Phys. Lett. **92**, 101913 (2008).
[19] V. Holý, U. Pietsch, and T. Baumbach, in *High Resolution X-ray Diffraction from Thin Films and Multilayers*, Tracts in Modern Physics Vol. 149, edited by G. Höhler (Springer, Berlin, 1999).
[20] Y. Tawara and K. Sato, J. Phys. Soc. Jpn. **18**, 773 (1963).
[21] G. Williamson and W. Hall, Acta Metall. **1**, 22 (1953).